Heliyon 9 (2023) e21521

Contents lists available at ScienceDirect

Heliyon

journal homepage: www.cell.com/heliyon

Effective chloride ion resistance of aluminum powder through interface electric field designing

Fei Wang [a,*], Lele Tong [b], Dan Li [a], Xinlin Wei [a], Jian Mao [a,**]

[a] College of Materials Science and Engineering, Sichuan University, Chengdu, 610065, China
[b] Sichuan Aerospace Chuannan Initiating Explosive Technology Limited, Luzhou, 646000, China

ARTICLE INFO

Keywords:
Nanoparticles
Nanocomposites
Interfacial electric field
Chloride ions
Density functional theory

ABSTRACT

Pure aluminium (Al) powder is widely used in aerospace fields as fuel while its corrosion mechanisms and anti-corrosion strategies are not thoroughly studied. Herein, corrosion mechanisms of Al nanoparticles are revealed by density functional theory (DFT) and experiments. Moreover, by utilizing the behaviour of ions moving in the electric field, an interfacial electric field is designed to endow spherical aluminium powder (sAl) with high anti-corrosion for chloride ions (Cl^-). Because TiO_2 presents lower electrostatic potential than Al_2O_3 which is on the surface of sAl, the prepared core@shell structural material (sAl@TiO_2) holds an interfacial electric field and its direction is from TiO_2 to Al_2O_3. The electric field repels the Cl^- adsorption on the surface of sAl@TiO_2, bringing about superior Cl^- anti-corrosion.

1. Introduction

Pure aluminium (Al) powder is widely used in aerospace fields as a kind of fuel [1,2]. During the preparation of fuel powder, the Al/Al-based powder is mixed with the perchlorate [3–5]. After prolonged storage, the activity of fuel powder would decrease or even lose efficacy, and it is critical to prevent Al powder from being corroded by Cl^-. Regarding the anti-corrosion of Al against Cl^-, current studies are focused on the bulk Al/Al-alloys [6–8], and works on the resistance to Cl^- of Al powder have not been studied yet and the corrosion mechanisms also are not clear.

Cl^- is a kind of anion, and it moves along the opposite direction of the electric field [9]. Learning from previous works, the interfacial electric field can be established between two surfaces with differential electrostatic potentials [10,11]. Generally, the Al_2O_3 layer would grow on the surface of Al nanoparticles. Theoretically, the interfacial electric field would be formed by introducing a coating layer which has a differential electrostatic potential [12]. If the electric field direction is from the coating layer to the Al_2O_3 layer, the electric field would repel the movement of Cl^- towards Al_2O_3 layer, preventing the Al powder from corroding.

In this work, the TiO_2 layer with lower electrostatic potential than that of Al_2O_3 is encapsulated on the surface of spherical Al (sAl) powder (sAl@TiO_2), and an electric field from TiO_2 to Al_2O_3 is established at the interface of TiO_2/Al_2O_3 heterostructure. The established interfacial electric field can effectively hinder the adsorption of Cl^-, and prevents the sAl from corroding. The corrosion production of sAl is $Al(OH)_3$ and mechanisms are studied by density functional theory (DFT) and experiments.

* Corresponding author.
** Corresponding author.
E-mail addresses: echo1994wf@foxmail.com (F. Wang), maojian@scu.edu.cn (J. Mao).

https://doi.org/10.1016/j.heliyon.2023.e21521
Received 24 August 2023; Received in revised form 18 September 2023; Accepted 23 October 2023
Available online 31 October 2023

2. Experiments and simulations

2.1. Experiments

A certain amount of titanyl sulfate was dissolved into 800 mL of deionized water to obtain solution A. Except for special instructions, the additive amount of titanyl sulfate was 0.3 g. The additive amount of titanyl sulfate can regulate the thickness of formed TiO_2. 1 g spherical sAl was added into solution A to react for 30 min. The obtained grey powder was sintered at 500 °C for 2 h in Ar to obtain the sAl@TiO_2.

The corrosion of powders (sAl and sAl@TiO_2) in perchlorate was simulated by immersing the powders into 3.5 wt% NaCl solution [13]. The phase structures were characterized by X-ray diffraction (XRD). Surface information was examined by X-ray photoelectron spectroscopy (XPS). The morphology and structures were tested by scanning electron microscopy (SEM) and transmission electron microscopy (TEM). The Al^{3+} concentrations of NaCl solutions at various time were tested by inductively coupled plasma optical emission spectroscopy (ICP-OES).

2.2. Simulations

DFT calculations were conducted in Dmol3 code (Materials Studio 2020) using Perdew–Burke–Ernzerhof (PBE) generalized gradient approximation (GGA) functional. The convergence criteria were maximal force of 0.003 Ha/Å, energy change of 1×10 Ha^{-5} and displacement of 0.001 Å. The Monkhorst–Pack grid k–points were set as $4 \times 5 \times 3$. The adsorption energy (E_{ad}) was calculated as following Equation [14].

$$E_{ad} = E_t - E_s - E_m \quad (1)$$

where E_t is the total energy of intermediates on the slab, E_s is the energy of slab and E_m is the energy of the intermediates.

3. Results and discussion

The X-ray diffraction (XRD) patterns (Fig. 1(a)) of sAl and sAl@TiO_2 well correspond to metal Al (standard card PDF#04–0787). Owing to that the amount of encapsulated TiO_2 is very small, the peaks regarding TiO_2 are absent in the XRD pattern of sAl@TiO_2. The size of sAl is around 4 μm and its surface of sAl is smooth observed by the SEM morphology (Fig. S1). For the sAl@TiO_2, the size is similar to the sAl and a thin layer around 5 nm can be observed on its surface (Fig. 1(b)–(c)). Learned from the selected area electron diffraction (SAED) pattern (Fig. S2), the centre sphere is crystalline metal Al which is consistent with the XRD results. The XPS Ti 2p spectrum of sAl@TiO_2 (Fig. 1(d)) can be deconvoluted into Ti $2p_{1/2}$ and Ti $2p_{3/2}$ indicating its feature of Ti^{4+} (TiO_2) [15], while the XPS Ti 2p signal (Fig. 1(e)) is absent for the sAl. Based on the energy dispersive spectroscopy (EDS) result, the content of Ti is around 0.18 at%. During EDS testing, the samples are pasted on the carbon conductive tape, and the signal of C stems from the carbon

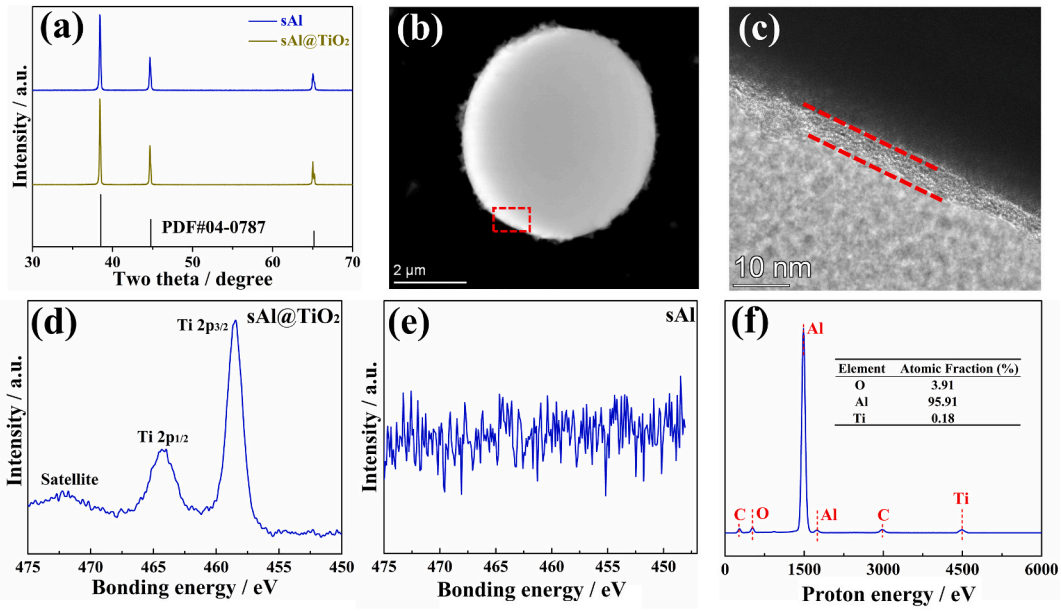

Fig. 1. (a) XRD patterns of sAl and sAl@TiO_2. **(b)** HAADF-STEM morphology of sAl@TiO_2 and **(c)** corresponding enlarged area (the red box) in (b). XPS Ti 2p spectra of **(d)** sAl@TiO_2 and **(e)** sAl. **(f)** EDS spectrum of sAl@TiO_2 and the contents of O, Al and Ti elements.

conductive tape. The above results indicate that a thin layer TiO_2 (around 5 nm) is encapsulated on the surface of sAl successfully.

The interfacial electric field is determined by XPS and DFT calculations. As shown in Fig. 2(a), all XPS Al 2p spectra present a peak at around 72 eV (Al^0, the peak also is set as calibration) and a peak at around 75 eV (Al^{3+}, Al_2O_3) [16]. The peak shift at around 75 eV in sAl@TiO_2 suggests the imbalanced charge distribution occurs at the heterointerfaces, forming the interfacial electric field [12,17,18]. The DFT calculations are employed to confirm the interfacial electric field. The (001) plane of TiO_2 and Al_2O_3 is established owing to the high stability (Fig. S3) [19]. The work functions of TiO_2 and Al_2O_3 are 7.90 eV and 6.06 eV respectively (Fig. 2(b)–(c)). The interfacial electric field (uniform charge distribution) is further confirmed by the charge density difference (Fig. S4). Compared with the isolated (001) plane of TiO_2 and Al_2O_3, the charge density difference presents an obvious imbalance [9]. Therefore, an interfacial electric field is established and its direction is from TiO_2 to Al_2O_3 (Fig. 2(d)) [9].

3.5 wt% NaCl solution is prepared to simulate the seawater and the solution is widely used to accelerate the corrosion process [20]. After the sAl is immersed in 3.5 wt% NaCl solution for 10 days, the metal Al phase is completely transferred to $Al(OH)_3$ (Fig. 3(a)) and the grey Al powder is changed into white $Al(OH)_3$ (insets). The Cl^- would attack and destroy the Al_2O_3 layer and sAl causing pitting, and the released Al^{3+} would react with the OH^- to produce $Al(OH)_3$ [6]. For the sAl@TiO_2, the phase still is the metal Al phase revealed by the XRD pattern (Fig. 3(b)) and the colour still is grey (metal sAl). After being immersed for 10 days, the peaks (XPS Al 2p spectrum) of sAl@TiO_2 are the same as that of primitive sAl@TiO_2 (Fig. 3(c)), indicating that the outer Al_2O_3 and inner metal Al still exist and the established interfacial electric field is also maintained. Because the sAl is completely transferred to $Al(OH)_3$, the XPS 2p spectrum only presents the peak of Al^{3+}. Te sAl has been completely dissolved and recrystallized into plate-like and strip-like $Al(OH)_3$ (Fig. 3(d)). Although the spherical sAl@TiO_2 suffers from a certain degree of corrosion, the shape and size of sAl@TiO_2 spheres remain constant substantially (Fig. 3(e)–**(f)**). The above result suggests that the interfacial electric field can effectively prevent the corrosion of sAl from Cl^-.

For corrosion procedures, the initial step is the intimate contact between materials and corrosion inducers [6]. For isolated TiO_2 and Al_2O_3, the E_{ad} for Cl^- is −1.01 eV and −1.57 eV respectively (Fig. 4(a)-(b)). For the TiO_2/Al_2O_3 heterostructure, the E_{ad} for Cl^- decreases to −0.62 eV (Fig. 4(c)). The E_{ad} is inversely proportional to adsorption strength. Therefore, the formed interfacial electric field hinders the adsorption of Cl^-. Because Cl^- is a kind of anion, it would move in the opposite direction of the electric field. Therefore, the formed electric field repels the adsorption of Cl^- on the surface of outer TiO_2 (Fig. 4(d)). To highlight the key role of the established electric field, sAl@TiO_2 with various thicknesses of TiO_2 layers is prepared by controlling the content of added titanyl sulfate (0.1 g, 0.3 g and 0.5 g). The higher the content of titanyl sulfate, the thicker the TiO_2 layer (Fig. 5(a)-(b)). These sAl@TiO_2 and sAl samples are immersed in 3.5 wt% NaCl solution for 1 day, and the concentrations of Al^{3+} tested by ICP-OES are shown in Fig. 5(c). It is clear that the thickness presents little effect on the anti-corrosion performance, and the corrosion resistance for Cl^- majorly comes from the interfacial electric field.

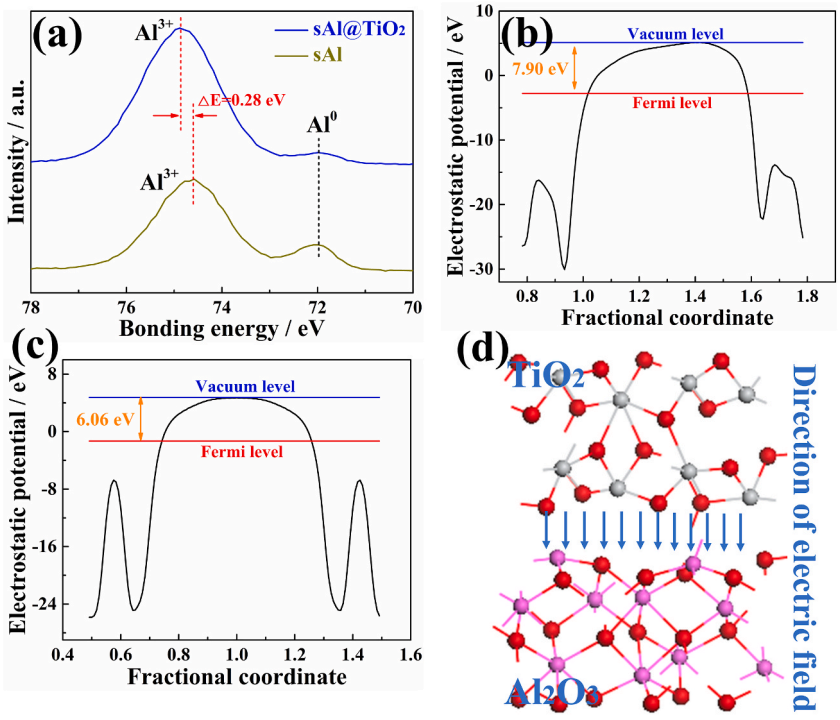

Fig. 2. (a) XPS Al 2p spectra of sAl and sAl@TiO_2. Electrostatic potential of **(b)** Al_2O_3 and **(c)** TiO_2 with exposed (001) planes. **(d)** Schematic of the formed electric field at the interface. The red, purple and grey spheres are O, Al and Ti atoms, respectively.

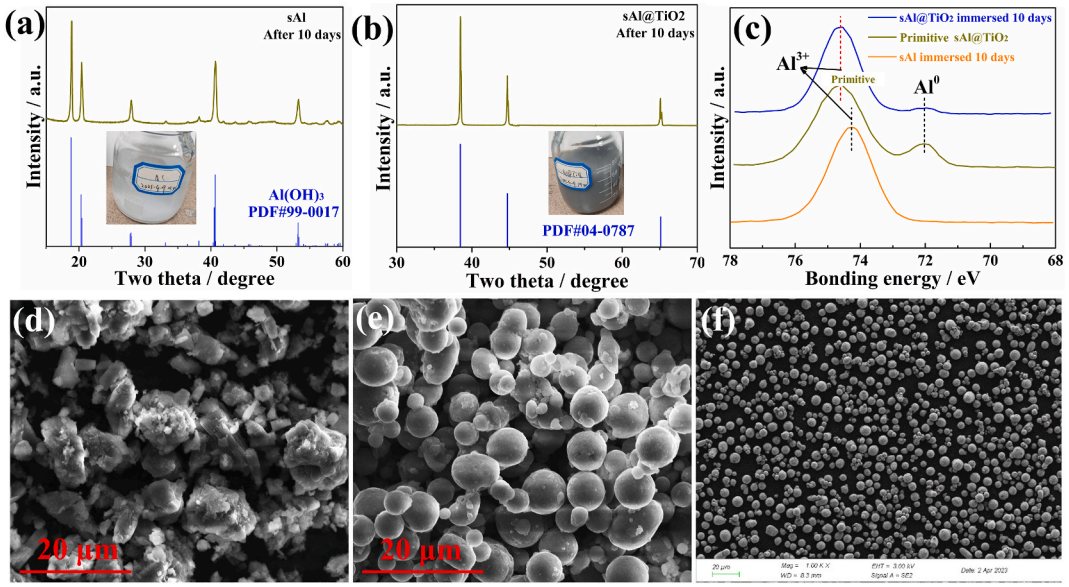

Fig. 3. XRD patterns of **(a)** sAl and **(b)** sAl@TiO_2 after 10 days of immersion. **(c)** XPS Al 2p spectra of sAl@TiO_2/sAl immersed for 10 days and primitive sAl@TiO_2. SEM morphology of **(d)** sAl and **(e)** sAl@TiO_2 after 10 days immersion. **(f)** SEM morphology of primitive sAl.

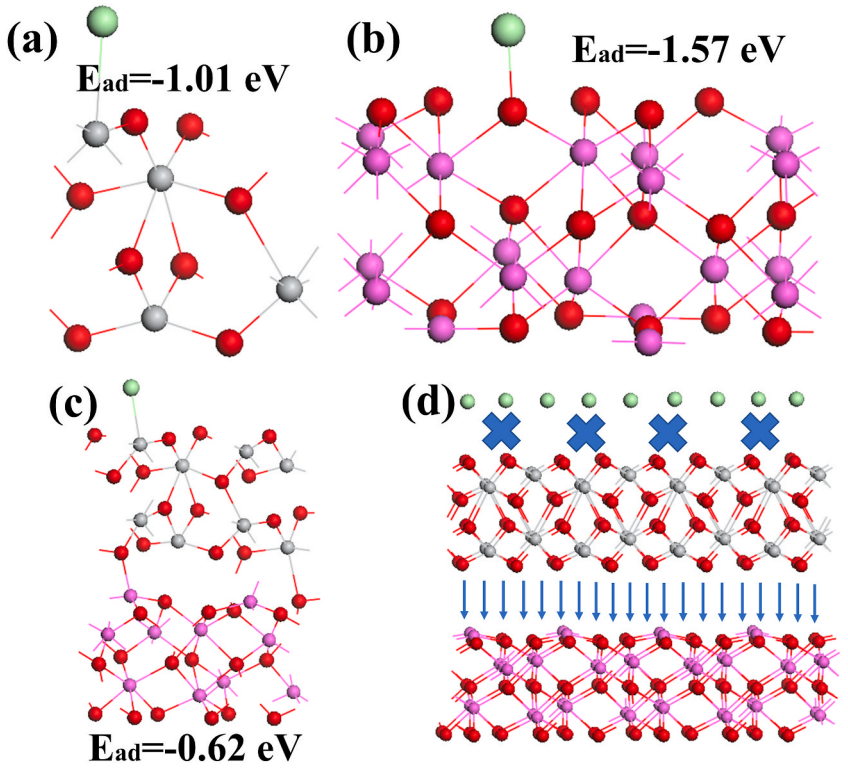

Fig. 4. Cl^- adsorbed on **(a)** TiO_2 (001), **(b)** Al_2O_3 (001) and **(c)** TiO_2/Al_2O_3 heterostructure, and corresponding E_{ad}. **(d)** Schematic of the formed interfacial electric field to hinder Cl^- adsorption. The green sphere is the Cl^-.

4. Conclusion

The core-shell structural sAl@TiO_2 is prepared and the heterostructural interface of TiO_2/Al_2O_3 is formed. Since TiO_2 present a lower electrostatic potential than Al_2O_3, an interfacial electric field is established and the direction is from TiO_2 to Al_2O_3. The anions

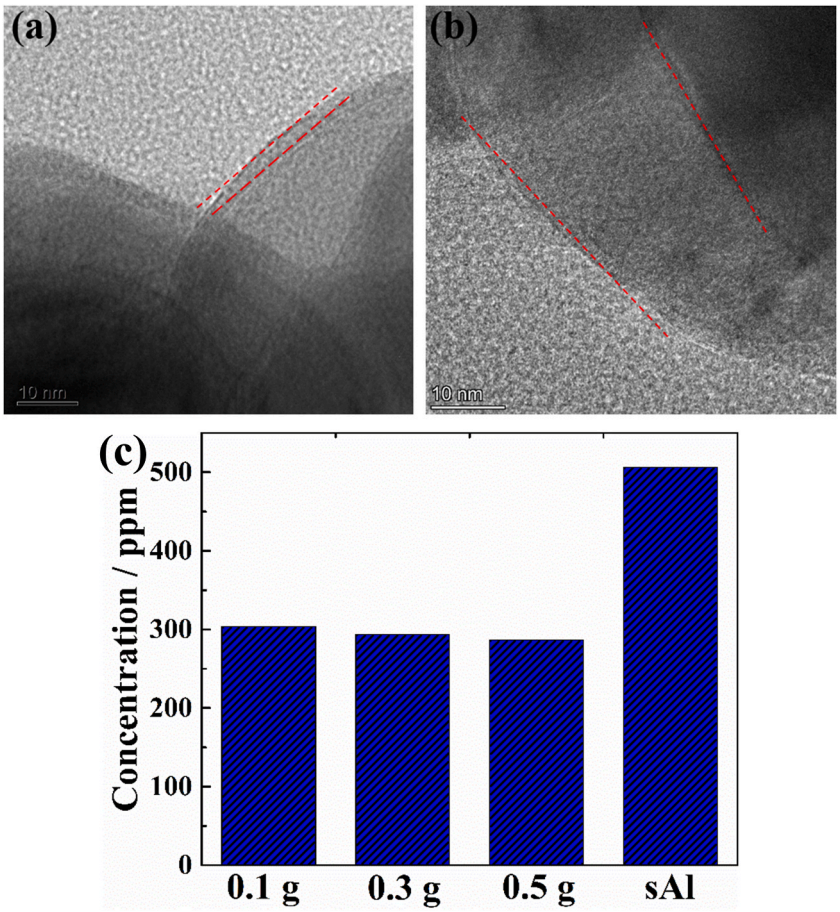

Fig. 5. TEM morphology of sAl@TiO_2, which is prepared by using **(a)** 0.1 g and **(b)** 0.5 g titanyl sulfate. The Al^{3+} concentrations of 3.5 wt% NaCl solution, when sAl@TiO_2 prepared by 0.1, 0.3 and 0.5 g titanyl sulfate (three on the left) and sAl are immersed for 1 day.

always move along the opposite direction of the electric field, therefore, the formed interfacial electric field repels the adsorption of Cl^-, decreasing the E_{ad} for Cl^-.

The prepared sAl@TiO_2 presents superior resistance for Cl^- corrosion. Immersing in 3.5 wt% NaCl solution for 10 days, the sAl (Al metal) completely transfers into $Al(OH)_3$, while the morphology and phase structure of sAl@TiO_2 still maintain almost constant. The formation of electric field from TiO_2 to Al_2O_3 and its repulsion effect for Cl^- are verified by DFT calculations and experiments. This work paves a new pathway for designing high-performance anti-corrosion materials by the interfacial strategy.

Credit authorship contribution statement

Fei Wang: Investigation, Formal analysis, Writing-original draft, Funding acquisition, Conceptualization, Visualization. **Lele Tong**: Resources. **Dan Li**: Investigation. **Xinlin Wei**: Writing. **Jian Mao**: Conceptualization, Resources, Supervision.

Data availability statement

Data will be made available on request.

Declaration of competing interest

The authors declare that they have no known competing financial interests or personal relationships that could have appeared to influence the work reported in this paper.

Acknowledgements

This work was supported by the [2021 Strategic Cooperation Project between Sichuan University and The People's Government of

Luzhou (2021CDLZ-1)], [the Fundamental Research Funds for Central Universities] and [Postdoctoral Research and Development Fund of Sichuan University (2023SCU12001)]. We would like to thank the Analytical & Testing Center of Sichuan University for providing the DFT simulation tools, and Shiyanjia Lab (www.shiyanjia.com) for the support of XPS tests.

Appendix A. Supplementary data

Supplementary data to this article can be found online at https://doi.org/10.1016/j.heliyon.2023.e21521.

References

[1] J. Yuan, J. Liu, et al., Acta Astronaut. 156 (2019) 14–22.
[2] Y. Zhou, J. Liu, et al., J. Therm. Anal. Calorim. 133 (2018) 1335–1344.
[3] K.V. Suresh Babu, P. Kanaka Raju, et al., Def. Technol. 13 (2017) 239–245.
[4] Y. Li, C. Hu, et al., Acta Astronaut. 133 (2017) 455–466.
[5] S. Elbasuney, A. Fahd, et al., Fuel 208 (2017) 296–304.
[6] F. Wang, J. Mao, Prog. Org. Coating 132 (2019) 191–200.
[7] Liu.M, C. Du, et al., Microstructures 3 (2023), 2023020.
[8] X. Huang, Q. Zhao, et al., Corrosion Sci. 216 (2023), 111089.
[9] F. Wang, J. Mao, ACS Appl. Mater. Interfaces 13 (2021) 13191–13199.
[10] S. Chen, F. Liu, et al., J. Cclloid. Interf. Sci. 553 (2019) 613–621.
[11] Y. Zheng, T. Zhou, et al., Angew. Chem., Int. Ed. 55 (2016) 3408–3413.
[12] T. Meng, B. Li, et al., ACS Nano 14 (2020) 7066–7076.
[13] X. Meng, X. Li, et al., J. Mol. Struct. 1253 (2022), 132279.
[14] F. Wang, J. Mao. Mater. Horiz. 10 (2023) 1780.
[15] C. Yan, Y. Zhu, et al., Adv. Funct. Mater. 28 (2018), 1705951.
[16] Y. Zheng, T. Zhou, et al., Angew. Chem., Int. Ed. 55 (2016) 3408–3413.
[17] Y. You, A. Ito, et al., Mater. Lett. 106 (2013) 11–13.
[18] W. Yuan, Y. Wang, et al., Nano Lett. 16 (2016) 132–137.
[19] C. Li, S. Dong, et al., Energy Environ. Sci. 11 (2018) 3201–3211.
[20] K. Shahzad, M. Sliem, R. Shakoor, et al., Sci. Rep-UK 10 (2020) 4314.